ACS APPLIED MATERIALS & INTERFACES

www.acsami.org

Research Article

Reprogrammable Soft Swimmers for Minimally Invasive Thrombus Extraction

Anna V. Pozhitkova, Daniil V. Kladko, Denis A. Vinnik, Sergey V. Taskaev, and Vladimir V. Vinogradov*

Cite This: ACS Appl. Mater. Interfaces 2022, 14, 23896−23908

Read Online

ACCESS | Metrics & More | Article Recommendations | Supporting Information

ABSTRACT: Thrombosis-related diseases are the primary cause of death in the world. Despite recent advances in thrombosis treatment methods, their invasive nature remains a crucial factor, which leads to considerable deadly consequences. Soft magnetic robots are attracting widespread interest due to their fast response, remote actuation, and shape reprogrammability and can potentially avoid the side effects of conventional approaches. This paper outlines a new approach to the thrombosis treatment via reprogrammable magnetic soft robots that penetrate, hook, and extract the plasma clots in a vein-mimicking system under applied rotating magnetic fields. We present shape-switching bioinspired soft swimmers, capable of locomotion by different mechanisms in vein-mimicking flow conditions and whose swimming efficiency is similar to animals. Further, we demonstrate the potential of a developed robot for minimally invasive thromboextraction with and without fibrinolytic usage, including hooking the plasma clot for 3.1 ± 1.1 min and extracting it from the vein-mimicking system under the applied magnetic fields. We consider an interesting solution for thrombosis treatment to avoid substantial drawbacks of the existing methods.

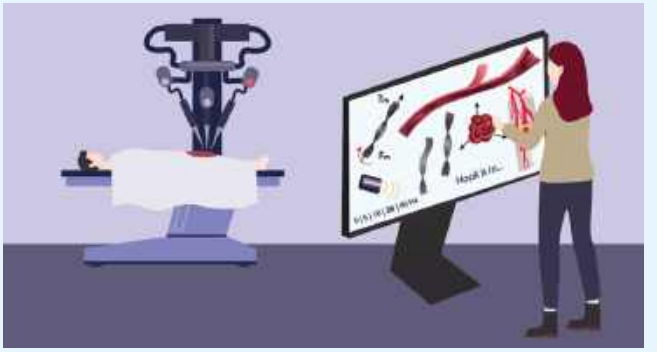

KEYWORDS: *medical soft robots, reprogrammable magnetization, untethered, thrombosis, minimally invasive surgery*

INTRODUCTION

One in four deaths worldwide is caused by ischemic heart disease and stroke collectively, according to the National Center for Health Statistics, 2017.[1] Thrombosis is one of the main etiological reasons for ischemic heart disease, stroke, and venous thromboembolism and leads to approximately half of all stroke deaths.[2]

Nowadays, the primary approach for thrombosis treatment remains surgery, which is based on mechanical thrombus extraction by catheter-based mechanical devices or another endovascular device like a balloon or stent.[3] However, despite the remarkable development of the minimally invasive system (MIS) for thrombosis treatment, its invasive nature and deadly side effects still have a substantial influence on the efficiency of therapy. The limitations of endovascular treatment include damage to venous valves and vessels caused by thrombectomy devices,[4] subarachnoid hemorrhages, distal emboli, intracranial dissections, and hematomas.[5] Although MIS methods have been applied in various fields of medicine and science[6−8] and even commercialized as clinically relevant research systems,[9] they are still limited by the scalability challenges, the rigidity of their components, and navigation and manipulation issues in limited and tortuous areas.[10−12]

In terms of thrombosis treatment development and avoiding side effects of the conventional methods, magnetically responsive soft materials attract considerable interest as untethered, complex, and fast shape-switching systems.[13−15] Moreover, the magnetic field can penetrate most materials, such as water, air, or a human body,[16,17] without energy dissipation and provides fast remote untethered operation control. Besides, the reduced stiffness allows great miniaturization of the surgical systems to reach the most suitable form for any operation and, therefore, better steerability.[18] Such magnetic systems provide essential properties for the medical field, such as tether-free actuation, necessary compliance, mechanical elasticity, adaptation to the outer surroundings,[19] and scalability, in contrast to conventional soft robotics devices in this field of study.[20,21] Recent findings regarding thrombosis therapy treatment have led to the development of the magnetic catheter navigation technique NiobeVR Magnetic Navigation System (Stereotaxis Inc., St. Louis),[22−24] which is more precise and effective due to the remote control of the operation. Nevertheless, it still uses the permanent magnets incorporated

Received: March 17, 2022
Accepted: April 25, 2022
Published: May 10, 2022

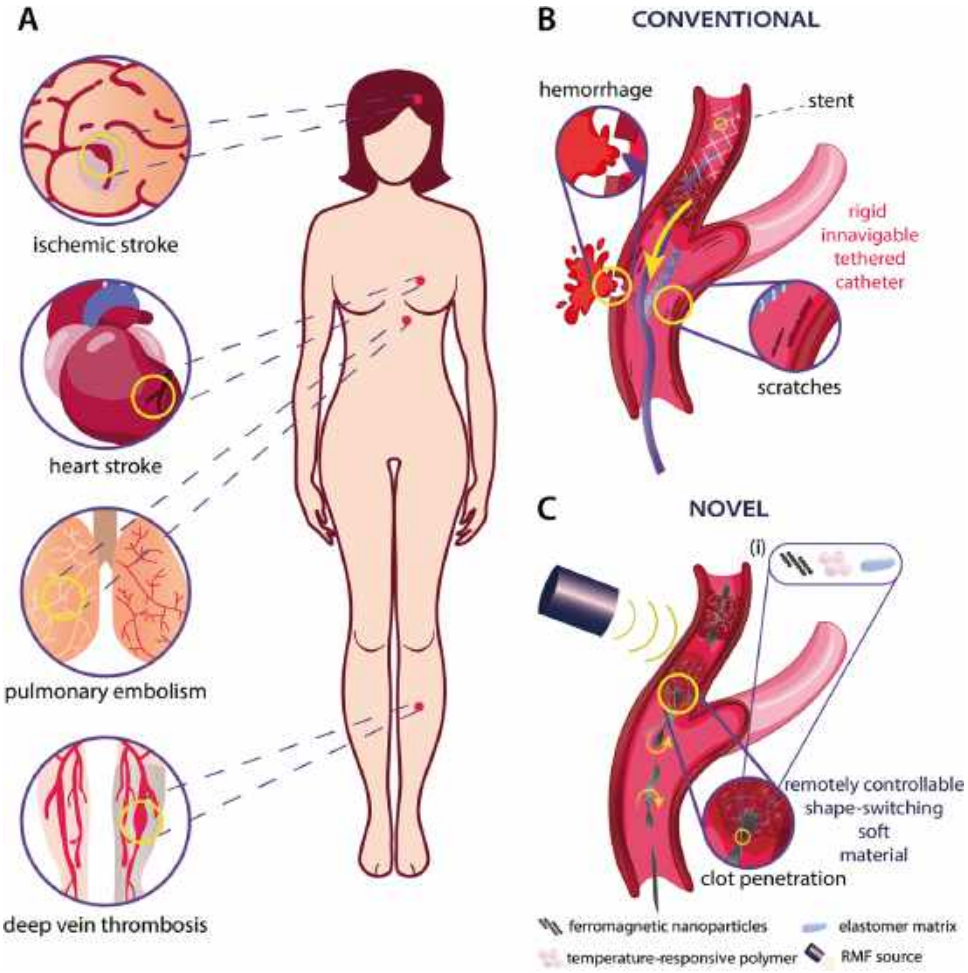

Figure 1. Schematic illustration of the ferromagnetic reprogrammable soft robot for thrombus extraction. (A) Pathologic thrombosis conditions in hard-to-reach areas across the human body where soft robots with active steering and navigating capabilities have utility, (B) illustration of the application of conventional thrombosis treatment and side effects of this therapy, and (C) illustration of the proposed concept of the active steerability of a soft robot navigating in a vein vessel and hooking the clot. (i) Composition of the soft reprogrammable magnetic robot. The legend is the inset.

in the catheter body, which limits this method and causes miniaturization and navigation challenges.[25]

Magnetically responsive soft materials could conceivably solve the above-mentioned issues, unlike the existing methods. These materials consist of soft matrices with embedded hard magnetic particles (in particular, hard neodymium−iron−boron (NdFeB) microparticles). The interaction between the magnetically induced torque and the internal mechanical force permits remote control of such systems. The main advantage of these materials is the magnetization programmability, which can change magnetic particle alignment during fabrication.[26,27] Applied magnetic fields generate torque on soft magnetic materials until the magnetization direction of all domains is aligned with the field direction.[28] However, the physical confinement of magnetic filler within the soft matrix with a permanent magnetization pattern limits the functional reconfiguration of soft devices for a wide range of applications. It requires the fabrication of the additional device for novel material features. The magnetic reprogramming technique is an attractive approach to improving soft material functionality where the magnetization pattern could be tailored by applying a magnetic field.[13,14,29,30] Although the presented advance shows the magnetization flexibility in one soft robot, the potential of the developed workflow for minimally invasive surgery has not been discussed and often provides only different proof-of-concept shape demonstrations.[31−34]

Herein, we demonstrate minimally invasive programmable magnetic soft robots for thrombus extraction *in vitro*. The programmability of the proposed robots, which is based on the physical rearrangement of the magnetization patterns in the soft matrix, is an essential factor for these soft materials. This process is enabled by the transition from a solid to liquid phase of the temperature-responsive polymer, which allows magnetic particles either to rotate freely or fix their positions in the matrix. Numerical tools were used for analyzing the transformation mechanism. Based on the theoretical framework, we have developed magnetization patterns of such soft materials by specially designed magnetic setups required for the reprogramming processes. Thus, three bioinspired designs of reprogrammable soft magnetic swimmers capable of navigating fluids were developed and tested in magnetic fields. Further, we analyzed the motion characteristics of our robots and demonstrated the capability of a soft swimmer to navigate through a vein-mimicking environment, penetrate the plasma clot under the rotating magnetic field (the field amplitude is 10

https://doi.org/10.1021/acsami.2c04745
ACS Appl. Mater. Interfaces 2022, 14, 23896−23908

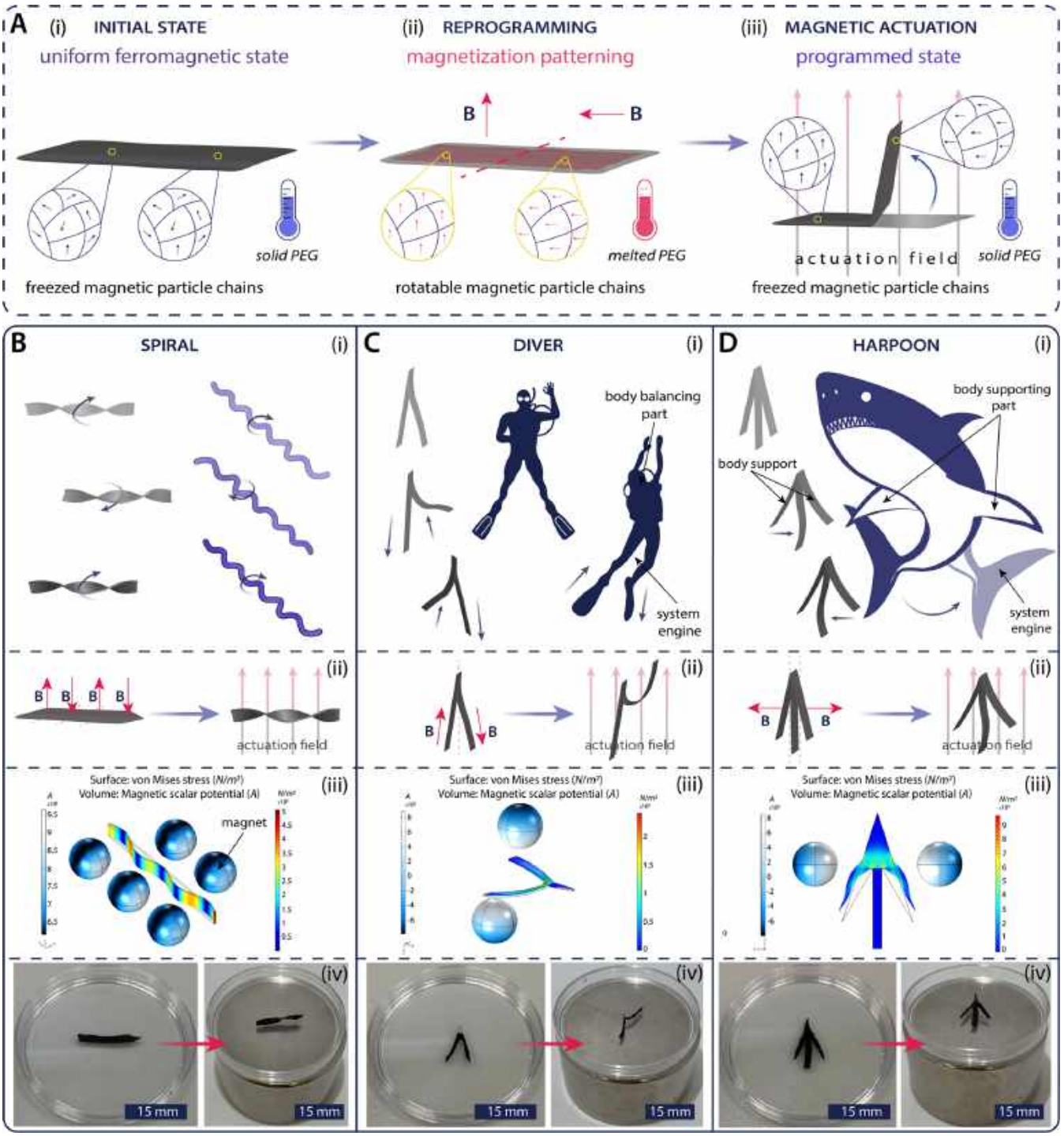

Figure 2. Reprogramming process for the magnetic soft robot. (A) Schematic illustration of the reprogramming process. (i) Initial state of the composite, (ii) reprogramming step, and (iii) magnetic actuation of the composite. (B–D) Illustration of three designs of magnetic robots, capable of navigating in fluid environments. (i) Bioinspired design of the magnetic robot, (ii) schematic illustration of the initial state of the proposed robots and their magnetic actuation under the applied magnetic field, (iii) numerical simulation of the magnetic soft robot deformation in the magnetic setups for the reprogramming process, and (iv) initial state of the magnetic soft robots and magnetic actuation of the obtained samples after the reprogramming process under the applied magnetic field.

mT, the field frequency is 40 Hz in X and Z directions), hook it for 3.1 ± 1.1 min, and extract it from the model vessel.

RESULTS

Robot Requirements. On the basis of research, we hypothesized the optimal properties of robots required to make the soft analogous interventional material that could avoid the conventional problem of such devices (see Figure 1). First, the soft nature of the robot (Young's modulus (E) ~ 0.01–1 MPa) is beneficial due to the increased steerability and effective navigation inside the blood vessel under external stimuli compared to a rigid device (E ~ 1–10 GPa). Moreover, the above-mentioned property also decreases the probability of hemorrhage and vessel scratch formation. Second, we

https://doi.org/10.1021/acsami.2c04745
ACS Appl. Mater. Interfaces 2022, 14, 23896–23908

suggested using a magnetic field as it is safe and allows the remote control of the robot even in human body scale[35−38] ($\nabla B \sim 30-100$ T/m) and helps make the untethered remotely controlled robot. This approach increases the maneuverability of the catheter and allows us to make the shape-switching robot via a reprogramming process with precise control in the vessel ($B \sim 10-100$ mT). The reprogramming process allows us to rewrite the original magnetization profile (uniform magnetization within the robot) after robot preparation to a new one, which is suitable for increasing locomotion activity of the robot. Finally, the application of the rotating magnetic field (RMF) (frequency of the magnetic field (f) $\sim$ 10−40 Hz) provides an opportunity to penetrate the fibrin mesh by the mechanical action of the magnetic soft robot and extract the thrombus from the blood vessel. It is also important to emphasize the biocompatibility of robot composition without using the relatively high-cost material.

To address the presented requirements, we propose a reprogrammable magnetic composite consisting of semihard magnetic iron−cobalt (FeCo) particles encapsulated in a temperature-responsive polymer (poly(ethylene glycol) (PEG)) embedded onto an elastomer matrix (see Figure 1C(i)). Unlike the common approaches, where the hard magnetic particles (in particular, neodymium−iron−boron (NdFeB) microparticles) are used, we present a new technique with magnetic semihard iron−cobalt (FeCo) nanoparticles, which possess higher saturation magnetization (M) and lower coercivity (for details, see the SI Section: Synthesis of Ferromagnetic Nanoparticles). The shape-anisotropic FeCo particles are also considered semihard magnetic materials[39,40] with promising properties for fabricating soft robots without the need for high cost, eco-unfriendliness, and toxic rare-based magnetic particles[41] from the robot design. The description of reaction mechanisms and detailed characterization of these particles are summarized in Supporting Information (Section 1: Characterization of the Particles).

The reprogramming process includes the phase transition from solid to liquid of a temperature-responsive polymer matrix. This transition allows rearranging the physical positions of magnetic particles according to applied fields. Therefore, we can change the magnetization profiles by heating the composite, applying magnetic fields in different directions, and cooling the composite below the melting temperature. As a temperature-responsive polymer, we suggest using poly(ethylene glycol) (PEG) 4000, as it is an appropriate candidate as an encapsulating material to conduct the reprogramming process due to its low melting temperature (58 °C) and comparatively low viscosity (114−142 mPa·s). For the elastomer matrix, we chose Ecoflex, which is widely used in diverse areas of soft robotics and medical fields due to its biocompatible composition, softness, and stretchability.[42,43]

Designs of Swimmers and the Reprogramming Process. Next, we introduce the shape-switching of the robot structure as a crucial advantage for minimally invasive surgery. These swimming robots in biomedicine are site-specific, stimuli-responsive devices to avoid the off-target influence on the undesirable processes during operation. Such body alternation under external stimuli was a challenge to be addressed. For this purpose, we adopted the previously published concept of the magnetic reprogramming process[44] with a novel magnetic filler and specially designed magnetic setups to control magnetization patterns within robots.

Figure 2A illustrates the reprogramming process of a soft magnetic robot for further experimental investigations of active navigation and thrombus extraction (see the SI Section: Reprogramming Process). Initially, the soft magnetic composite is in a uniform ferromagnetic state, which is attributed to the continuous random direction of the magnetization (Figure 2A(i)). This state is assumed as frozen with a negligible variation of the ferromagnetic particles within the elastomer matrix due to the low viscosity of the PEG (114−142 mPa·s). The next step includes heating the composite above the melting temperature (58 °C) of the encapsulated polymer and applying the necessary magnetic fields to get the required magnetization directions after the reprogramming process (Figure 2A(ii)). Increasing PEG fluidity above the melting point allows the ferromagnetic particle reorientation upon magnetic field application. Thus, the whole magnetization pattern of the composite can be divided into many parts and changed in the desired way. The last step of the reprogramming process is cooling the composite and, therefore, fixing the magnetization pattern and magnetic actuation of the reprogrammed material into the designed form (Figure 2A(iii)).

Following the specific requirements and main task to create the minimally invasive soft swimmers, we present three designs of our ferromagnetic soft robots, capable of navigating in fluid environments (see Figure 2B(i)−D(i)). Such designs of the robots were selected based on the concept of the complex bioinspired structures with active locomotion. The corresponding parameters for design also include the length-actuation part spacing ratio (L/S) selected equal to $L/S \sim 4$ to ensure the preferential for locomotion (for "spiral" and "diver") and $L/S \sim 2$ for body supporting ("harpoon").[45] The mimicry of the well-known swimming behavior corresponds to the head−tail morphology and lateral undulatory locomotion (*Spirulina* sp. and nematode) for the "spiral" form,[46] the "diver" form—bipedalism locomotion (e.g., human or penguin),[47] and the "harpoon" form—a streamline body with locomotion supported by lateral fins (e.g., shark).[48] The robot's size corresponds to the dimensions of the veins[16] and is approximately $10 \times 2 \times 0.2$ mm^3.

To reprogram the forms and get the necessary design for the subsequent analysis of their steerability in the fluid surroundings, specially designed magnetic setups with desired distributions of magnetic fields were used (Figure S2A−C). The reprogramming should include the transformation of the original strip into the "spiral" (Figure 2B(ii)), the "diver" could alternate the leg position for swimming (Figure 2C(ii)), and the "harpoon" opens fins for body support and locomotion by the rest of the body (Figure 2D(ii)). The design of magnetic setups and subsequent analysis of robot deformation were performed in COMSOL Multiphysics 5.5. The setups were made of spherical magnets with a diameter of 4 and 5 mm and organic glass molds, which were implemented by the milling cutter (see Figure S2D−F).

Figure 2B(iii)−D(iii) presents the calculated magnetic scalar potential of magnetic force density and deformation of the magnetic soft body for each setup (see the Supporting Information Section 2: Finite Element Analysis of the Bioinspired Robots). As for the "spiral" form, the design of the magnetic setup includes the nonsymmetric spatial organization of magnets to ensure the alternation of magnetic field gradient maximum and minimum (Figure 2B(iii)). This field topology establishes that the interaction between a

https://doi.org/10.1021/acsami.2c04745
ACS Appl. Mater. Interfaces 2022, 14, 23896−23908

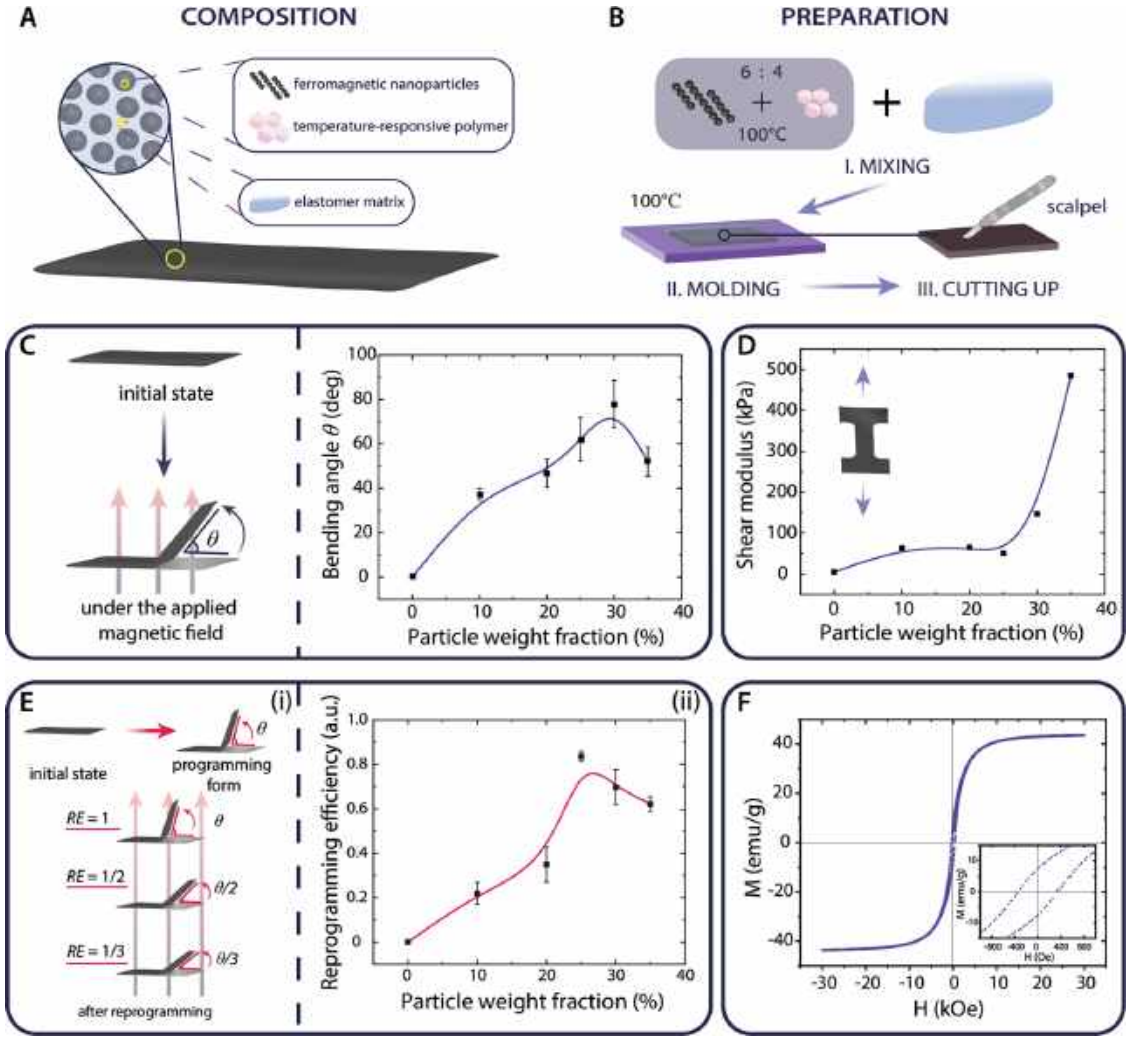

Figure 3. Magnetic soft composite characterization. (A) Composition of the soft magnetic robot, (B) preparation method of the soft magnetic robot, (C) experimental data of obtained bending angle measurements, (D) composite mechanical testing, and (E) reprogramming efficiency (RE) measurements. (i) Schematic illustration of the RE concept and (ii) experimental data of the obtained RE. (F) Room-temperature magnetic hysteresis loop of the composite with the particle concentration at 30 wt %.

magnetic composite and spherical magnets is repulsive in the low magnetic field gradient region and attractive in the high magnetic field gradient region, resulting in the folding of the magnetic robot in a spiral-like structure. The magnetic setup for the "diver" form consists of two magnets located vertically relative to each other and producing attractive interaction between one magnet and one end of the robot (Figure 2C(iii)). Such a field topology leads to the separation of each "leg" of the "diver" to the opposite sides along the vertical axis; the nonmagnetic end performs as a weight stabilizer for this system. In the case of the "harpoon" form, the magnetic setup contains two magnets located horizontally relative to each other (Figure 2D(iii)). There is an attractive interaction between each magnet and the end of the robot close to it. Thus, the field topology of this setup results in the separation of the "fins" into opposite sides. The presented deformations for each magnetic robot proved the successful design of the magnetic setup and matched with functional bioinspired analogues.

Figure 2B(iv)–D(iv) presents the real samples after the reprogramming process under the applied field. The permanent magnet was used to establish whether the programming process changes the composite form under the external magnetic field after the reprogramming process. According to the multiphysical modeling, the magnetic robot folded into a predesigned form upon magnetic field application. The developed designs of the robots and magnetic setups for their reprogramming process allow getting forms capable of active steering in fluid environments under the applied rotating magnetic field.

Robot Composition and Characterization. The next research step was dedicated to finding the optimal robot composition required for efficient locomotion in the fluid environment and minimally invasive thromboextraction. The fabrication process of the composite started with mixing the ferromagnetic annealed magnetic particles with melted PEG in a 6:4 weight ratio and grinding them (see Figure 3B). Then, this mixture was blended with a silicone elastomer matrix at a 1:1 weight ratio and cured at 100 °C for 40 min in a mold. The solidified composite was peeled off from the mold, cooled, and cut into the designed patterns by scalpel (for details, see the SI Section: Composite Preparation). The surface morphology of the composite was examined by SEM and energy dispersive X-ray (EDX) analysis (see Figure S3). The distribution of FeCo

https://doi.org/10.1021/acsami.2c04745
ACS Appl. Mater. Interfaces 2022, 14, 23896−23908

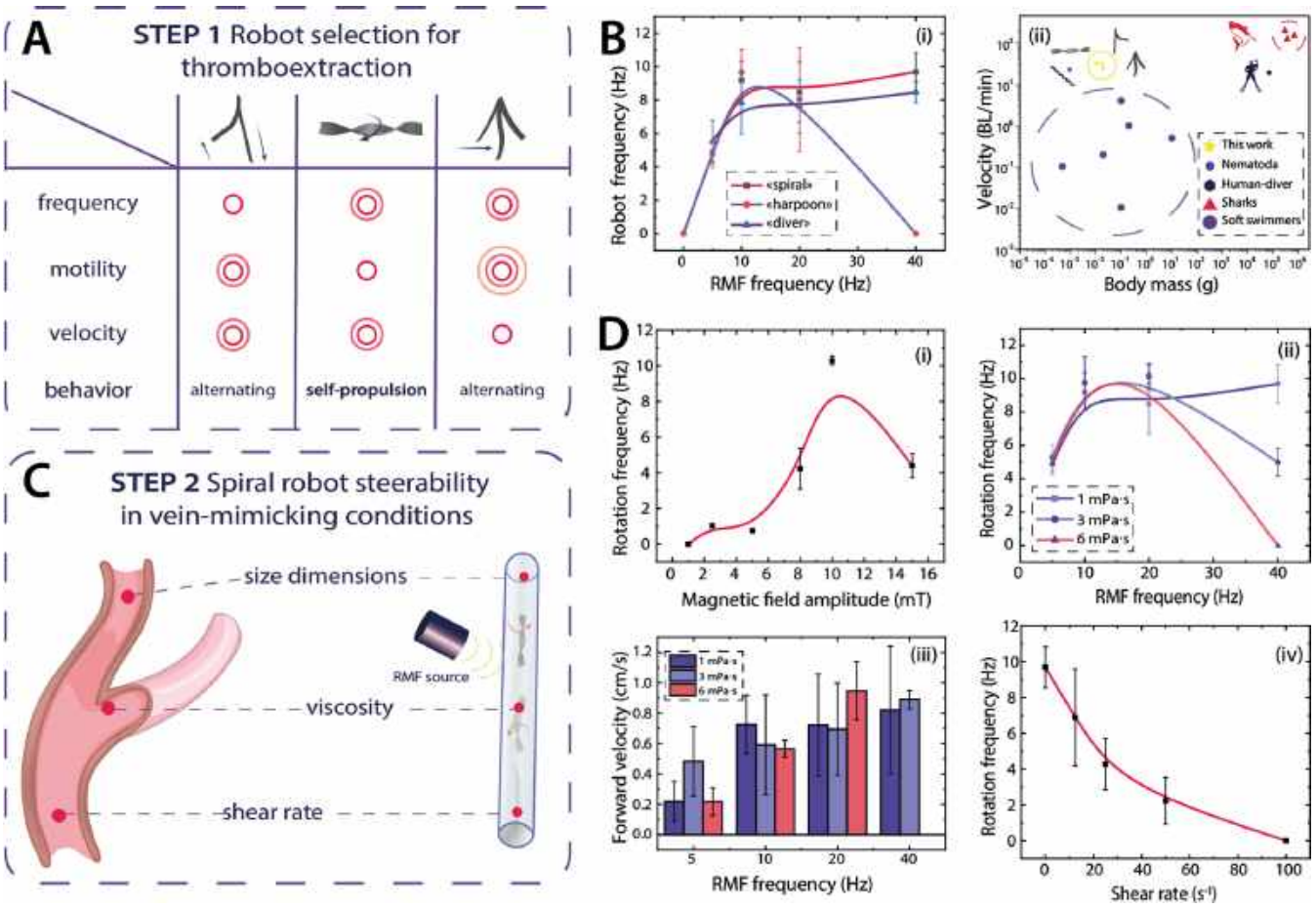

Figure 4. Active steering and navigation of the developed swimmers. (A) Robot selection for thromboextraction in regard to their motion characteristics and (B) rotating characteristics of the developed robots. (i) Robot frequencies in regard to the RFM frequency and (ii) summary of the swimming performances of organisms and artificial soft swimmers. (C) Experimental scheme for estimating the steerability of the robots and its comparison with the vein conditions and (D) rotating characteristics of the "spiral" robot under the applied RMF. (i) Dependence of the rotation frequency in regard to the magnetic field amplitude, (ii) experimental data of the rotating frequency of the "spiral" robot in distinct fluid viscosities, (iii) experimental data of the forward velocity of the "spiral" robot in distinct fluid viscosities, and (iv) dependence of the rotation frequency regarding the flow shear rate.

particles, PEG, and the silicon matrix was analyzed by mapping their characteristic elements. According to the EDX analysis, there was iron (Fe), cobalt (Co), silicon (Si), and carbon (C) in the composition. Due to the surface layer scanning by the EDX detector, there was a discontinuous distribution of Si elements from the elastomer matrix in the EDX images. Nevertheless, the elastomer matrix is, in fact, continuously distributed in the composite, as can be seen from the SEM image.

To estimate the required composition for maximizing the magnetic actuation performance, we measured the bending angle of the magnetic robot with different magnetic particle concentrations (Figure 3C). The actuation performance was measured by the magnetic composite bending angle under the external magnetic field, managing the magnetic particle concentration from 0 to 35 wt % with a fixed elastomer matrix concentration of 50 wt % in each composite (see the SI Section: Bending Angle Measurement). Figures 3C and S4B show a clear dependence on the magnetic actuation capability concerning the FeCo nanoparticle concentration in the case of crystalline and amorphous samples, respectively. It can be seen from the plots (see Figures 3C and S4B) that composites with crystalline particles show more significant magnetic response (with the bending angle maximum at 78 ± 10.6°) in contrast to the composites with amorphous particles (with the bending angle maximum at 42 ± 8.7°) at every particle volume fraction. In the case of the crystalline sample, the bending angle reaches its peak when the particle volume value is equal to 30 wt %.

To evaluate the mechanical properties of the magnetic composite, uniaxial tensile tests were performed on a mechanical testing machine (see the SI Section: Mechanical Testing Measurement). Figure 3D illustrates the shear modulus determined by fitting the experimental curve of nominal stress−stretch to a hyperelastic Mooney−Rivlin 2-parameter model. According to these results, it can be outlined that the most suitable volume fraction of a particle is from 30 and 35 wt %, at which point the shear modulus is about 150 and 485 kPa. The shear modulus increase is attributed to particle-mediated reinforcement of the elastomer matrix in the medium range of filler fraction.[49] The decrease in the bending angle value could be explained from a dimensionless parameter $\frac{MB}{G}$ (where M is magnetization (A/m), B is the magnetic flux density (T), and G is the shear modulus (Pa)), which shows the ratio between magnetic and mechanical properties of the robot (Figure S4C). The ratio reached the maximum at 25 wt

https://doi.org/10.1021/acsami.2c04745
ACS Appl. Mater. Interfaces 2022, 14, 23896−23908

% ($\frac{MB}{G} = 0.13$) with a decrease at 30 wt % ($\frac{MB}{G} = 0.053$) and minimum at 35 wt % ($\frac{MB}{G} = 0.018$).

To estimate the composite capability to be reprogrammed and perform the programmed forms under the applied magnetic field, the reprogramming efficiency (RE) value was introduced and analyzed with regard to the particle volume fraction (see the SI Section: Reprogramming Efficiency Measurement). The actuation performance was measured as the ratio between the programmed lifting angle of the composite and the obtained angle under the applied magnetic field, with the magnetic particle concentration ranging from 0 to 35 wt % with a fixed elastomer matrix concentration of 50 wt % in each composite (see Figure 3E(i)). Figure 3E(ii) presents the RE of the magnetic composite with the peak value (RE = 0.83 ± 0.02) at a particle fraction of 25 wt % with a slight decrease (RE = 0.69 ± 0.07) at 30 wt %. Nevertheless, we have chosen the magnetic composite for further analysis with a 30 wt % particle fraction in favor of a compromise between the shear modulus (150 kPa for 30 wt % and 50 kPa for 25 wt %) and the reprogramming efficiency value. Furthermore, as illustrated in Figure S4A, the value of RE is significantly lower for a composite with amorphous particles and reaches its peak only at 0.5, which implies the significant contribution of coercivity to the reprogramming process.

Further, the magnetic properties of the composite with the magnetic crystalline particle concentration at 30 wt % were analyzed by a SQUID magnetometer (see Figure 3F). The SQUID analysis shows the well-pronounced ferromagnetic behavior with coercivity (335.73 Oe), saturation magnetization (43.2 emu/g), and remanent magnetization (7.6 emu/g). The decrease in the obtained characteristics compared to the particle is attributed to the presence of an elastomer and polymer matrices that cover the particles.

Taken together, we analyze the magnetic and mechanical properties of two types of magnetic fillers (crystalline and amorphous FeCo). The results suggest the feasibility of crystalline semihard FeCo nanoparticles for magnetic soft robot fabrication, actuation, and reprogramming. For further study of magnetic robot behavior in fluid flow and for the thromboextraction task, we chose the magnetic composite with a 30 wt % particle fraction with a high shear modulus (150 kPa), highest actuation capability (bending angle reached 78 ± 10.6°), and good reprogramming efficiency (0.69 ± 0.07 a.u.).

Active Steering and Navigation. Hereafter, we demonstrate the capability of our magnetic soft robot for navigating in a vessel-mimicking system based on active steering and targeting upon the rotating and gradient magnetic fields, respectively. To select the most efficient robot for the swimming and thrombus extraction task, we propose several parameters (Table S1 and Figure 4A), including motility U (eq S2),[50] length-normalized velocity v (eq S3, body length (BL)/min),[51] shear modulus of robots tip G (kPa), movement frequency f, and behavior (Hz). These parameters allow us to estimate swimming efficiency and the probability of fibrin mesh penetration (for more details, see eqs S2 and S3 in SI). Initially, the motion characteristic of the designed magnetic soft robots in the presence of the RMF was estimated (Figure 4B and Movie S1).

The analysis of the three different robot form frequencies implied a distinct movement characteristic: "spiral" showed the self-propelled behavior and reached the maximum rotating frequency (9.69 ± 1.14 Hz) under a 40 Hz frequency of the external magnetic field. In contrast, the "harpoon" and "diver" showed the absence of rotation frequency. According to the programmed design, the relatively fast movement was achieved by alternating the swimming part of the robots' structure (Figure 4B(i)). The comparable frequency characteristic (8.46 ± 0.62 Hz for the "diver" and 9.67 ± 1.36 Hz for the "harpoon" at 40 and 10 Hz frequency of RMF, respectively) showed the effectiveness of the chosen bioinspiration strategies and magnetic programming design. The similar frequency-dependent behavior for "spiral" and "diver", contrary to "harpoon", might correspond to the geometry-affected viscous drag coefficient.[52]

The efficiency of developed swimmers could be described by two key parameters: motility U (the ratio of velocity to length and actuation frequency) and normalized velocity of the soft robots (in body length (BL)/min scale). The analysis of motility suggests that the "harpoon" with shark-like swimming performance (42.6 for the "harpoon" and 28.5 and 13.68 for the "diver" and the "spiral", respectively) had a higher energy efficiency conversion of the magnetic field torque in the swimming with similar U for the natural swimmer (e.g., *E. coli* has a $U \sim 30$[50]) and the artificial propeller and bioinspired microswimmer ($U \sim 40$ for the head-to-tail microswimmer[53]). Notably, the comparable motility of the magnetic soft robots reached significantly higher body size and weight.

The effective performance of these magnetic soft robots is demonstrated by comparing their normalized velocity against the body mass with that of the selected for bioinspiration animals (nematode, sharks, human-diver) and reported soft swimmers,[54] as presented in Figure 4B(ii). Surprisingly, the developed magnetic robots showed a higher swimming velocity (32.85 BL/min for "spiral" (0.82 cm/s), 25.57 BL/min (0.63 cm/s), and 34.2 BL/min (0.57 cm/s) for the "harpoon" and the "diver", respectively) than all previously reported soft robots with a comparable body weight. Moreover, their swimming performance was quite close to bioinspired examples such as nematodes (22.8 BL/min) and human beings with diver equipment (20.4 BL/min) but still lower than that for sharks (238.1 BL/min for *Isurus oxyrinchus*, 148.1 BL/min for *Carcharodon carcharias*, and 142.2 BL/min for *Galeocerdo cuvier*[55]).

Despite the significant swimming efficiency of three bioinspired designs, we have chosen the "spiral" form for minimally invasive thrombus extraction and the following characterization. The reason for this choice is the motion behavior of soft robots: we assume that "spiral" self-propulsion is beneficial because of the higher mechanical contact with a fibrin mesh compared to the mechanical influence of the alternating actuator ("diver" and "harpoon"). Moreover, the bioinspired mechanism of the "harpoon" movement could only push the fibrin clot, while the "spiral" changes the center of the mass after clot penetration and self-propels in another direction suitable for thrombus removal from the vessel. Notable is the fact that the higher shear modulus G of the sharp robot tip for the "spiral" (150 kPa) also increases the mechanical action on the biopolymer surface compared to the "diver" one (20 kPa) (see Table S1).

Next, we studied the rotating characteristics under the RMF action in different frequencies and amplitude conditions, viscosity, the shear rate of fluid, and the possibility of magnetic targeting of the soft robot (Figure 4C,D). The parameters of the tube and the flow rate (Q) replicate the human vein system with a 2.5 mm radius tube (r) and a vein wall shear rate (γ) in

https://doi.org/10.1021/acsami.2c04745
ACS Appl. Mater. Interfaces 2022, 14, 23896−23908

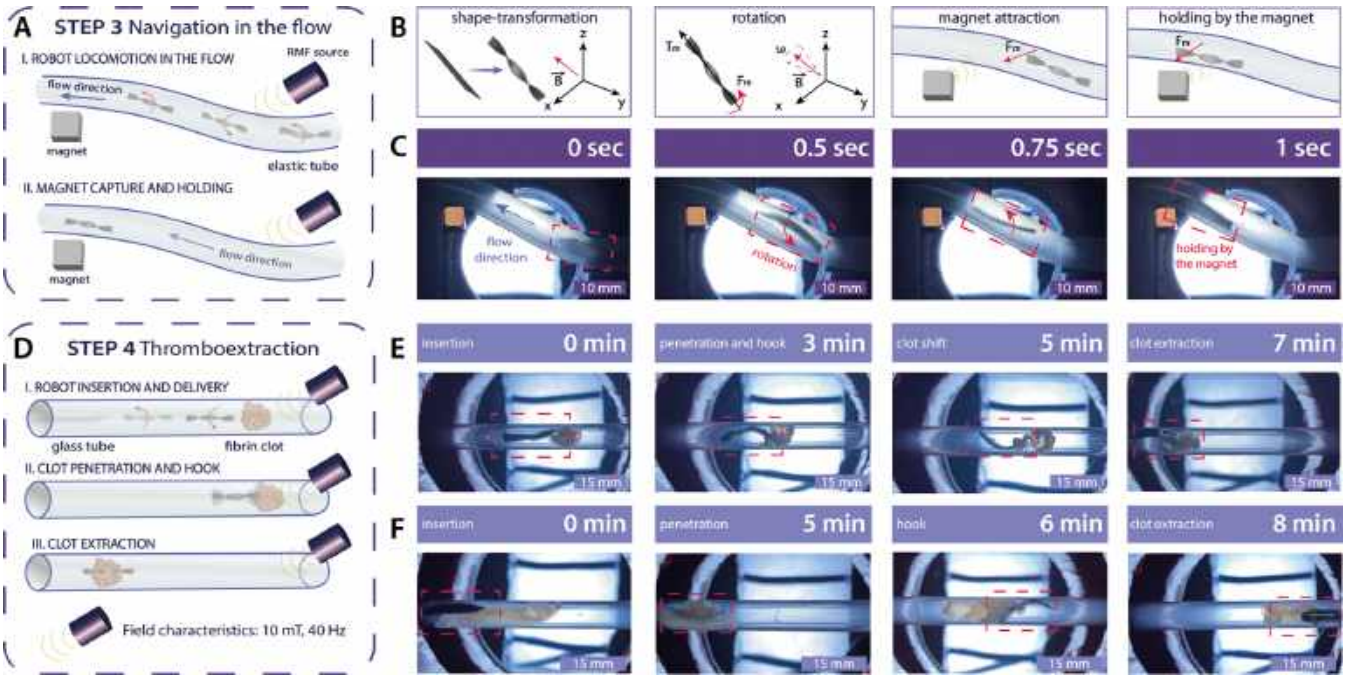

Figure 5. Applicability of the "spiral" robot for thromboextraction. (A) Experimental scheme for estimating the navigation of the "spiral" robot in the flow conditions, (B) theoretical model of the mechanisms of the robot rotation and capture, (C) navigation of the "spiral" robot in the flow and its capture and holding by the permanent magnet, (D) experimental scheme for the thromboextraction, and (E, F) experimental data on the realization of the main steps of the thromboextraction without and with thrombolytics, respectively.

the range of 15−200 s^{-1} by the equation[56] $\gamma = \frac{4Q}{\pi r^3}$ (Figure 4C). The frequency−amplitude analysis shows the optimal actuation parameters at a 10 mT magnetic flux density (Figure 4D(i)) and a 40 Hz RMF frequency (Figure S5). The significant change in the rotation frequency after the maximal synchronized point of both the frequency and the amplitude was observed and corresponded to the asynchronous and oscillation movement mode after the step-out frequency point (Movie S2).[57]

Figure 4D(ii,iii) show the differences in the robot rotating frequency and the velocity in different fluid viscosities, namely, similar to water (1 mPa·s), blood in arteria (3 mPa·s), and blood in a vein (6 mPa·s) (see SI Section: Preparation of Fluids).[58] The rotation and forward velocity characteristics were similar for the whole viscosity range in a 5−20 Hz actuation mode. However, with a magnetic field frequency of 40 Hz, we observed a drastic decrease in the rotation frequency, from half of the robot frequency in water for arterial blood viscosity (9.7 ± 1.14 Hz for 1 mPa·s and 5 ± 0.8 for 3 mPa·s) to the absence of rotation for vein blood viscosity. The increase of viscosity leads to attenuation of self-propulsion by viscous forces, which also shifts the step-out frequency of the magnetic soft robot.[52]

Figure 4D(iv) demonstrates the capability of a soft robot to rotate under the flow with different shear rates (see the SI Section: Vein-Mimicking System). The result presents a significant decrease in robot rotation frequency with an increase in the shear rate of the fluid. Specifically, we observed the twofold fall of frequency (4.3 ± 1.4 Hz) when the shear rate reached 20 s^{-1} and the absence of any rotation at 100 s^{-1}. Nevertheless, the developed soft robot has a remarkable rotation frequency in the 0−25 s^{-1} range suitable for navigation and active steering in the vein. Moreover, the magnetic soft swimmer can resist and locomote against the flow with a shear rate at ∼10 s^{-1}, a lower boundary of the vein shear rate (Movie S3).

The next research stage was to understand whether the ferromagnetic soft robot could be targeted and captured by a gradient magnetic field in the flow conditions (see Figure 5A−C). The experimental setup in Figure 5A consists of an elastic tube, a peristaltic pump, a permanent magnet, and Helmholtz coils (see the SI Section: Vein-Mimicking System). Figure 5B shows the main steps of robot actuation: the shape transformation and robot rotation due to the torque force from RMF and robot attraction and capturing by the gradient magnetic field. The snapshots in Figure 5C show the capability of the soft robot to move uniformly with the flow (0 s), rotate under the action of the rotating magnetic field (0.5−0.75 s), and be captured by a permanent magnet ($\nabla B \sim 50$ T/m) under the flow conditions. Moreover, after being captured, the magnetic soft swimmer could resist the flow with a velocity parameter of ∼15.5 cm/s (Movie S4). These results provide the perspective of the developed ferromagnetic robot for magnetic targeting of the occlusion region in the human-mimicking flow system during surgical operations. Taken together, the presented results demonstrate the robot's capacity to rotate under the viscous flow conditions being captured and navigated by the gradient magnetic field, which provides a blueprint for a new way of thrombosis treatment.

Thrombus Extraction Tasks. Our study provides further evidence for the capabilities of the proposed ferromagnetic soft robot for thrombus extraction (Figure 5D−F). As illustrated in Figure 5D, the experimental setup consists of a vein-mimicking glass tube, model plasma clots (see the SI Section: Preparation of Model Clots), and a rotating magnetic field setup (for details, see the SI Section: Rotating Magnetic Field Setup).

The concept of the experiments is the penetration of the clot by the programmed magnetic soft robot under the action of

https://doi.org/10.1021/acsami.2c04745
ACS Appl. Mater. Interfaces 2022, 14, 23896−23908

the rotating magnetic field (the field amplitude is 10 mT, the field frequency is 40 Hz in X and Z directions), using the screwing technique,[6,7,59] and then the unaided extraction of the swimmer with the clot from the vein-mimicking system due to the self-propelled nature of the material (see the SI Section: Thrombus Extraction Experiments). The snapshot in Figure 5E and Movie S5 demonstrates the main steps of the thromboextraction without thrombolytics: the insertion of the robot into the vein-mimicking tube (0 min), penetration and hook of the model fibrin clot (3 min), and further extraction of the clot from the vessel by self-propulsion of the swimmer with the hooked clot (5 and 7 min). The hook of the thrombus is the primary step and determines whether the robot could deliver the clot from the vessel by either self-propulsion of the robot itself or the gradient magnetic field with 3.1 ± 1.1 min (Figure S6) average time of the hook. It should be noted that in 10 repetitions, only in 5 cases out of 10 the successful thrombus hook and extraction were observed. There are two reasons for possible robot failure for thrombus extraction applications: the heterogeneity of the system and the magnetic control system. It is important to note that we did not observe the thrombus fall off the robot in the case of experiments without thrombolytics. The absence of thrombolytic drugs in the system avoids the main limitations of such drugs, such as systemic fibrinolysis and consequent hemorrhagic stroke.[60,61] Moreover, the soft nature of the robot is also beneficial for the conventional problem of rigid mechanical thrombectomy devices with tissue damage.

Nevertheless, the absence of thrombolytic drugs limits the ability of the developed swimmer to penetrate the thrombus due to a complex fibrin mesh with high mechanical stability.[62] To prove this suggestion, the experiments with a tissue plasminogen activator (t-PA) as a thrombolytic drug with a concentration of 4.3 mg/mL were performed (Figure 5F). Such a concentration was chosen according to the patient dose used during catheter surgery.[63] The snapshots from Figure 5F and Movie S6 show the complete penetration of the model fibrin clot by a magnetic robot, which corresponds to the fibrinolytic-mediated softness of the thrombus during thrombolysis.[64] Still, we observed no significant change in the clot hook time during drug-assisted thromboextraction (approx. 4 min). These results suggest that the clot hook without thrombolytics was strong enough to hold the clot and extract it from the model system without the mandatories of complete clot penetration. It is worth noting that the use of thrombolytic drugs increases the probability of thrombus uncoupling during the thromboextraction (Movie S7). It can be explained by thrombus dissolution under the action of thrombolytics and subsequent decrease in the mechanical stability of the clot. Therefore, we demonstrated the ability to extract thrombus from vein-mimicking vessels under the action of the rotating magnetic field due to the optimal design and fabrication of the ferromagnetic reprogrammable swimmer. The complete remote control of the actuator and the noninvasive nature of the magnetic field are valuable advantages of the presented system as a safe approach for the fabrication of renewed minimally invasive surgical devices.

DISCUSSION AND CONCLUSIONS

In this paper, we have developed the bioinspired reprogrammable magnetic soft swimmer, which possesses excellent navigating and manipulating characteristics and offers a great potential for biomedical applications in close and limited areas. We have optimized a methodology of magnetic soft composite preparation and programming to get any desired form of material under the applied external magnetic field. The theoretical framework based on analytical expressions and the multiphysical model predicted the optimal material composition and magnetic setup for the predesigned shape transformation of the ferromagnetic actuator. In our view, this approach constitutes a great initial step toward further translation and adaptation of the fabricated robot for minimally invasive surgery concepts in future medical practice.

Although our investigations so far have only been on a small scale, we illustrate a minimally invasive approach for thrombosis treatment in vein-mimicking conditions *in vitro* and highlight the potential of the developed magnetic soft robot for preclinical and clinical studies. This research has thrown up many questions in need of further examination, including the tests of vessel tissue damage, blood-contact issues, and extraction of the *ex vivo* blood clots. We believe that the application of the mechanical force-based extraction with a high loading rate of the actuator[65,66] could potentially improve the clot permeability for drugs and, consequently, decrease the mechanical stability of the fibrin mesh and increase the clot penetration probability by the developed system. Nevertheless, it is worth noting that the blood clots have several factors, such as age, blood cell composition, the shear rate of vessels, and clot size,[67] which determine the therapy inefficiency by thrombolytic drugs. Furthermore, according to the obtained experimental data, thrombolytics usage could potentially lead to the thrombus uncoupling from the robot due to the thrombus dissolution under the action of thrombolytics and in addition mechanical impact from robot rotation. In addition, the thrombolytics usage could the reason for the thrombus migration and reformation of the blood clot. Therefore, the development of the standardized methodology for robot preparation and reprogramming parallel with a magnetic setup with the precise coupling of gradient and rotating magnetic field[43] will increase the effectiveness of thrombus extraction by a magnetic soft robot.

Thus, the perspective of the application of the automated digital magnetic actuation systems[38] in surgery can be conceivably hypothesized from insertion applying minimally invasive procedures to complex navigation and operation under the action of the gradient and rotating magnetic field. The robot composition, including the ferromagnetic particles with high saturation magnetization, demonstrates magnetic targeting capability in a moderate magnetic field gradient range (~50−100 T/m), which could avoid the traditional problem of the magnetic field-mediated transport of robots.[25] The temperature-responsive polymer within the robot allows us to conduct the reprogramming process by the functional reconfiguration of soft devices and fabrication of the modular structure with different surgical parts.[32] Applying the artificial intelligent-based framework[68,69] and a powerful theoretical base and multiphysical modeling[27,70] could eventually lead to a new stage for magnetic soft robotics, namely, the rational inverse material design for minimally invasive surgery needs. Future studies should aim at the conventional visualization system as angiographic with radiopaque particles in the composite for preclinical and clinical trials.[71] We believe that combining all of these technologies could probably foster the development of the universal surgical platform for a wide range of interventional procedures.

https://doi.org/10.1021/acsami.2c04745
ACS Appl. Mater. Interfaces 2022, 14, 23896−23908

Finally, we have demonstrated our proof-of-concept study confirming the feasibility and performance of the robot in the vein-mimicking system for thromboextraction. We hope the present findings might help to develop a biomedical device under remote control for applications ranging from simple tasks to minimally invasive medical procedures.

MATERIALS AND METHODS

Materials. Iron(II) chloride tetrahydrate ≥98.5%, sodium borohydride, pyrrole, poly(ethylene glycol) (PEG) 4000, and cobalt(II) nitrate hexahydrate ≥98% were purchased from Sigma-Aldrich. Ecoflex 00-30 was purchased from Smooth-On Inc. Platelet-free lyophilized normal human plasma (PFP) and thrombin were purchased from Technologia Standart (Russia). Alteplase (Actilyse) was purchased from Boehringer Ingelheim International GmbH (Germany). Sucrose was purchased from NevaReaktiv, Russia. For all applications, deionized water (18 MΩ) was used (Millipore).

Synthesis of Ferromagnetic Nanoparticles. Amorphous magnetic particles were prepared as follows. First, the necessary amount of $FeCl_2{\cdot}4H_2O$ (0.135 g), $Co(NO_3)_2{\cdot}6H_2O$ (0.173 g), and C_4H_5N (0.750 mL) was dissolved in distilled water (20 mL). Meanwhile, $NaBH_4$ (0.650 g) was dissolved in distilled water (10 mL) and added dropwise into a solution of precursor salts during vigorous stirring (300 rpm). The reaction process would last for approximately 20 min until the precipitate fell.

Finally, the black precipitates were washed several times with distilled water and gathered by an external magnet. After that, the particles were freeze-dried for 6 h to get the final products.

To investigate the coercivity effect on the programming process, the synthesized sample was annealed under Ar gas flow at a temperature of 550 °C for 10 min. The obtained powders were collected for the following characterization.

Characterization of Ferromagnetic Particles before and after Annealing. The obtained powders were characterized by scanning electron microscopy (SEM) using a VEGA3 TESCAN scanning electron microscope, transmission electron microscopy (TEM) using a high-resolution TEM JEOL JEM 2200FS, and the X-ray diffraction analysis (XRD) on an Apex Duo (Bruker) at 1.5418 Å (Cu Kα). Magnetic properties were measured on a VersaLab Quantum Design magnetometer.

Reprogramming Process. The reprogramming process was prepared by adapting the procedure used by Song et al.[44] For this procedure, we used specially designed magnetic setups with desired distributions of magnetic fields. To estimate the magnetic properties of each setup for the programming process, COMSOL Multiphysics 5.5 software was used. The setups were made of spherical magnets with diameters of 4 and 5 mm and molds from organic glass, which were implemented by the milling cutter. The programming codes for the milling cutter were written by commercially available software package ArtCAM 2008.

The reprogramming process consists of several stages. First, we heat the composite to the melting temperature of the PEG to cause the phase transition; thus, our ferromagnetic particle chain can rotate freely in the matrix. Then, we apply magnetic fields in different directions to the composite, putting our composite in specially designed magnetic setups with different distributions of magnetic fields (see Figure S2) to obtain the necessary magnetization patterns in the soft material. Since our ferromagnetic particle chains are in the rotatable state, the magnetic domains easily rearrange in directions of applied fields. After that, our composite cools below the melting temperature of the phase change polymer; PEG is solid and, therefore, the magnetic domains are fixed, according to the applied fields.

To establish how the programming process changes the composite form, a permanent neodymium (NdFeB) disc magnet with dimensions 45 × 25 mm^2 was used.

Composite Preparation. The magnetic composite was prepared as follows. First, we heated poly(ethylene glycol) (PEG) to 100 °C above its melting temperature (58 °C) for about 3 min until the transition to the liquid phase. Then, we mixed the ferromagnetic annealed iron−cobalt (FeCo) nanoparticles with melted PEG in a 6:4 weight ratio and ground this compound into a powder. After that, this mixture was blended with a silicone elastomer matrix (Ecoflex 00-30) at a 1:1 weight ratio. The mixture was poured onto a mold and cured at 100 °C for 40 min on magnetic stirring. The mold has a rectangular shape with an aspect ratio of 20 × 10 × 0.3 mm^3. The solidified composite was peeled off from the mold and cooled. The obtained composite was cut into the designed patterns by a scalpel.

Characterization of the Composite. Magnetic properties were measured on a VersaLab Quantum Design magnetometer. The specimens with different particle volume fractions were tested on a mechanical testing machine (Metec, LS1) with a 20 N load cell at a strain rate of 0.01 s^{-1}. The surface morphology of the composite was analyzed by scanning electron microscopy (SEM) using a TESCAN MIRA scanning electron microscope (Czech Republic). The ionic cut was performed using equipment SEMPrep2 (Technoorg Linda, Hungary). The energy dispersive X-ray (EDX) analysis was done using an EDS Ultim (Oxford Instruments, Great Britain).

Bending Angle Measurement. Composites with magnetic particle concentrations from 0 to 35 wt % were prepared. One-half of each composite was fixed with an elastic band, while the bending angle of another half under the applied field was measured. The external magnetic field is generated by a rectangular-shaped neodymium−iron−boron (NdFeB) permanent magnet, whose dimensions are 120 × 80 × 20 mm^3. A series of experiments with different magnetic particle concentrations were carried out. The resulting angle was calculated in ImageJ free software (NIH).

Mechanical Testing Measurement. Soft composites with different magnetic particle concentrations (0, 10, 20, 25, 30, and 35 wt % magnetic particle concentrations) were prepared by molding in the dog bone-shaped patterns with assigned dimensions (width, 5 mm; gauge length, 20 mm; thickness 0.8 mm). The molds were implemented by a milling cutter, for which the programming code was written by a commercially available software package ArtCAM 2008. The samples were tested on a mechanical testing machine (Metec, LS1) with a 20 N load cell at a strain rate of 0.01 s^{-1}. The nominal stress−stretch curve was plotted for each sample, and the shear modulus was determined by fitting the experimental curve to a Mooney−Rivlin 2-parameter model, using the WELSIM software application. Material constants were obtained from the curve-fitting on the experimental strain−stress data and then used for the shear modulus calculation and the hyperelasticity modeling in COMSOL Multiphysics 5.5 software. The shear modulus G was calculated accordingly to the equation

$$G = 2(c_{10} + c_{01}) \quad (1)$$

Reprogramming Efficiency Measurement. Composites with magnetic particle concentrations from 0 to 35 wt % were prepared. All composites were programmed following these steps: First, the composite was heated above the melting temperature of the encapsulated polymer (PEG). Next, it was shaped into the desired form under an external magnetic field and cooled while applying the field to fix the magnetic domains. In this case, our desired form is the uplift to 90° of one-half of the composite under an external magnetic field. The external magnetic field is generated by a rectangular-shaped neodymium−iron−boron (NdFeB) permanent magnet, whose dimensions are 120 × 80 × 20 mm^3. A series of experiments with different magnetic particle concentrations were carried out. The resulting angle was calculated in ImageJ free software (NIH).

Preparation of Fluids. Three fluids with viscosities similar to water (1 mPa·s), arterial blood (3 mPa·s), and vein blood (6 mPa·s), consisting of sucrose in different concentrations, were prepared to investigate the motion characteristics of the "spiral" form. The concentration of sucrose in the case of arterial blood (3 mPa·s) was 50 mg/mL; for the vein blood (6 mPa·s), this value was 69 mg/mL. The viscosities of obtained fluids were measured by the EXPERT rotational viscometer model from Fungilab, SA.

Vein-Mimicking System. The experimental scheme consists of an elastic tube (the length is 60 cm, the diameter is 5 mm), a pump (Pump Drive PD 5101, Heidolph Instruments GmbH & Co. KG,

https://doi.org/10.1021/acsami.2c04745
ACS Appl. Mater. Interfaces 2022, 14, 23896−23908

Germany), and two chemical glasses. The deionized water was constantly pumped through the tube system with the adjusted parameters of pumping at 120, 60, 30, and 15 rpm, which correspond to the 100, 50, 25, and 12.5 s^{-1} shear rates, respectively. The "spiral" robot was placed in the glass tube with the same pumping conditions.

The second experiment was dedicated to the capability of the magnetic soft catheter to be held by a permanent magnet against and in the flow. For this experiment, the permanent neodymium (NdFeB) magnet cube magnet with dimensions 4 × 4 mm^2 was used. The composite was placed in the elastic tube, where the flow velocity was 15.5, 7.5, 3.75, and 1.8 cm/s, respectively.

Preparation of Model Clots. The fibrin clots for experiments were prepared following the next steps: mixing equal volumes of platelet-free normal human plasma (prepared from lyophilized powder according to specification) with a thrombin solution (4 IU/mL) and leaving for about 1 min in ambient conditions.

Rotating Magnetic Field Setup. A rotating magnetic field (RFM) was created using a custom-built TOR 3D device ("Nanomaterials", Russia). This equipment is composed of three pairs of axially positioned Helmholtz coils that can produce magnetic fields in different directions. There is a uniform field in each chamber with the maximum magnetic flux density in the center of the experiment chamber being 15 ± 2% mT. It is possible to use two or three to use two out of three pairs of coils simultaneously to make a rotating magnetic field. The frequency can be adjusted in the range of 1−200 Hz with a 0.1 Hz step and the amplitude ranging from 1 to 15 mT with a 0.1 step.

Thrombus Extraction Experiments. An experimental setup includes a rotating magnetic field setup, a vein-mimicking glass tube with a diameter of 5 mm and a length of 20 cm, and the model plasma clots. The experiments were carried out with a thrombolytic concentration of 4.3 mg/mL and without it. Alteplase was used as a thrombolytic, which is a tissue plasminogen activator. The magnetic soft catheters were prepared and programmed as discussed earlier (for details, see the SI Section: Reprogramming Process). The dimensions of catheters were 15 × 2 × 0.3 mm^3 and the catheter had a pointed end to realize a thrombus hook more effectively.

The experiments proceeded following the steps outlined below. At first, the model clot was prepared as discussed earlier (for details, see the SI Section: Preparation of Model Clots). Then, the clot and a programmed magnetic soft material prepared in advance were placed in the tube with one closed end. Hereafter, the distal water or thrombolytic was added to the tube and the other end of it was closed by parafilm to prevent the leakage of the liquid. This tube was inserted in a rotating magnetic field setup TOR 3D with adjusted parameters: the field amplitude was 10 mT and the field frequency was 20 Hz in *X* and *Z* directions. The experiments were continued from 4 to 10 min till the clot was not hooked by the magnetic soft catheter and extracted.

■ ASSOCIATED CONTENT

Supporting Information

The Supporting Information is available free of charge at https://pubs.acs.org/doi/10.1021/acsami.2c04745.

Designed forms, capable of navigating in fluids (Movie S1) (MP4)

Step-out frequency point of the "spiral" form (Movie S2) (MP4)

Navigation of the "spiral" form against the flow (Movie S3) (MP4)

Navigation of the "spiral" form in and against the flow, held by the permanent magnet (Movie S4) (MP4)

Thromboextraction experiment without thrombolytics (Movie S5) (MP4)

Thromboextraction experiment with thrombolytics (Movie S6) (MP4)

Thrombus uncoupling from the robot body (Movie S7) (MP4)

Structural characterization of obtained particles (Figure S1); magnetic setups for the reprogramming process (Figure S2); EDX mapping of the composite (Figure S3); characterization of the magnetic soft composite with amorphous particles (Figure S4); rotating characteristics of the "spiral" form under the applied RMF (Figure S5); hook time of the thromboextraction experiments without thrombolytics (Figure S6); and comparison of bioinspired ferromagnetic robots (Table S1) (PDF)

■ AUTHOR INFORMATION

Corresponding Author

Vladimir V. Vinogradov − *International Institute "Solution Chemistry of Advanced Materials and Technology", ITMO University, St. Petersburg 197101, Russia;* orcid.org/0000-0002-5081-4876; Email: vinogradov@scamt-itmo.ru

Authors

Anna V. Pozhitkova − *International Institute "Solution Chemistry of Advanced Materials and Technology", ITMO University, St. Petersburg 197101, Russia*

Daniil V. Kladko − *International Institute "Solution Chemistry of Advanced Materials and Technology", ITMO University, St. Petersburg 197101, Russia*

Denis A. Vinnik − *National Research South Ural State University, Chelyabinsk 454080, Russia*

Sergey V. Taskaev − *National Research South Ural State University, Chelyabinsk 454080, Russia; Chelyabinsk State University, Chelyabinsk 454001, Russia*

Complete contact information is available at: https://pubs.acs.org/10.1021/acsami.2c04745

Funding

The work was financially supported by the Russian Science Foundation no. 21-73-10150. The authors also thank Priority 2030 Federal Academic Leadership Program for infrastructure support.

Notes

The authors declare no competing financial interest.

■ ACKNOWLEDGMENTS

X-ray powder diffraction studies were performed on the Rigaku SmartLab 3 diffractometer of the engineering center of the Saint-Petersburg State Technological Institute (Technical University). The energy dispersive X-ray (EDX) analysis of the composite was carried out at the TESCAN demonstration laboratory in St. Petersburg. The authors thank A. Prilepskii (ITMO University, Russia) for proofreading the manuscript.

■ REFERENCES

(1) Heron, M. Deaths: Leading Causes for 2017. *Natl. Vital Stat. Rep.* **2019**, *68*, 1−77.

(2) Raskob, G. E.; Angchaisuksiri, P.; Blanco, A. N.; Buller, H.; Gallus, A.; Hunt, B. J.; Hylek, E. M.; Kakkar, A.; Konstantinides, S. V.; McCumber, M.; Ozaki, Y.; Wendelboe, A.; Weitz, J. I. Thrombosis: A Major Contributor to Global Disease Burden. *Arterioscler., Thromb., Vasc. Biol.* **2014**, *34*, 2363−2371.

(3) Vedantham, S.; Goldhaber, S. Z.; Julian, J. A.; Kahn, S. R.; Jaff, M. R.; Cohen, D. J.; Magnuson, E.; Razavi, M. K.; Comerota, A. J.; Gornik, H. L.; Murphy, T. P.; Lewis, L.; Duncan, J. R.; Nieters, P.;

Derfler, M. C.; Filion, M.; Gu, C.-S.; Kee, S.; Schneider, J.; Saad, N.; Blinder, M.; Moll, S.; Sacks, D.; Lin, J.; Rundback, J.; Garcia, M.; Razdan, R.; VanderWoude, E.; Marques, V.; Kearon, C. Pharmacomechanical Catheter-Directed Thrombolysis for Deep-Vein Thrombosis. *N. Engl. J. Med.* **2017**, *377*, 2240−2252.
(4) Ali, A.; Sakes, A.; Arkenbout, E. A.; Henselmans, P.; van Starkenburg, R.; Szili-Torok, T.; Breedveld, P. Catheter Steering in Interventional Cardiology: Mechanical Analysis and Novel Solution. *Proc. Inst. Mech. Eng., Part H* **2019**, *233*, 1207−1218.
(5) Goktay, A. Y.; Senturk, C. Endovascular Treatment of Thrombosis and Embolism. *Adv. Exp. Med. Biol.* **2017**, *906*, 195−213.
(6) Lee, S.; Lee, S.; Kim, S.; Yoon, C.-H.; Park, H.-J.; Kim, J.; Choi, H. Fabrication and Characterization of a Magnetic Drilling Actuator for Navigation in a Three-Dimensional Phantom Vascular Network. *Sci. Rep.* **2018**, *8*, No. 3691.
(7) Jeon, S. M.; Jang, G. H. Precise Steering and Unclogging Motions of a Catheter with a Rotary Magnetic Drill Tip Actuated by a Magnetic Navigation System. *IEEE Trans. Magn.* **2012**, *48*, 4062−4065.
(8) Hu, X.; Chen, A.; Luo, Y.; Zhang, C.; Zhang, E. Steerable Catheters for Minimally Invasive Surgery: A Review and Future Directions. *Comput. Assisted Surg.* **2018**, *23*, 21−41.
(9) Vitiello, V.; Lee, S.-L.; Cundy, T. P.; Yang, G.-Z. Emerging Robotic Platforms for Minimally Invasive Surgery. *IEEE Rev. Biomed. Eng.* **2013**, *6*, 111−126.
(10) Vitiello, V.; Lee, S. L.; Cundy, T. P.; Yang, G. Z. Emerging Robotic Platforms for Minimally Invasive Surgery. *IEEE Rev. Biomed. Eng.* **2013**, *6*, 111−126.
(11) Gopesh, T.; Wen, J. H.; Santiago-Dieppa, D.; Yan, B.; Pannell, J. S.; Khalessi, A.; Norbash, A.; Friend, J. Soft Robotic Steerable Microcatheter for the Endovascular Treatment of Cerebral Disorders. *Sci. Rob.* **2021**, *6*, No. eabf0601.
(12) Li, J.; De Ávila, B. E. F.; Gao, W.; Zhang, L.; Wang, J. Micro/Nanorobots for Biomedicine: Delivery, Surgery, Sensing, and Detoxification. *Sci. Rob.* **2017**, *2*, No. eaam6431.
(13) Hu, W.; Lum, G. Z.; Mastrangeli, M.; Sitti, M. Small-Scale Soft-Bodied Robot with Multimodal Locomotion. *Nature* **2018**, *554*, 81−85.
(14) Kim, Y.; Yuk, H.; Zhao, R.; Chester, S. A.; Zhao, X. Printing Ferromagnetic Domains for Untethered Fast-Transforming Soft Materials. *Nature* **2018**, *558*, 274−279.
(15) Wu, S.; Ze, Q.; Zhang, R.; Hu, N.; Cheng, Y.; Yang, F.; Zhao, R. Symmetry-Breaking Actuation Mechanism for Soft Robotics and Active Metamaterials. *ACS Appl. Mater. Interfaces* **2019**, *11*, 41649−41658.
(16) Nelson, B. J.; Kaliakatsos, I. K.; Abbott, J. J. Microrobots for Minimally Invasive Medicine. *Annu. Rev. Biomed. Eng.* **2010**, *12*, 55−85.
(17) Ceylan, H.; Giltinan, J.; Kozielski, K.; Sitti, M. Mobile Microrobots for Bioengineering Applications. *Lab Chip* **2017**, *17*, 1705−1724.
(18) Runciman, M.; Darzi, A.; Mylonas, G. P. Soft Robotics in Minimally Invasive Surgery. *Soft Rob.* **2019**, *6*, 423−443.
(19) El-Atab, N.; Mishra, R. B.; Al-Modaf, F.; Joharji, L.; Alsharif, A. A.; Alamoudi, H.; Diaz, M.; Qaiser, N.; Hussain, M. M. Soft Actuators for Soft Robotic Applications: A Review. *Adv. Intell. Syst.* **2020**, *2*, No. 2000128.
(20) Rich, S. I.; Wood, R. J.; Majidi, C. Untethered Soft Robotics. *Nat. Electron.* **2018**, *1*, 102−112.
(21) Charreyron, S. L.; Gabbi, E.; Boehler, Q.; Becker, M.; Nelson, B. J. A Magnetically Steered Endolaser Probe for Automated Panretinal Photocoagulation. *IEEE Rob. Autom. Lett.* **2019**, *4*, 284−290.
(22) Yuan, S.; Holmqvist, F.; Kongstad, O.; Jensen, S. M.; Wang, L.; Ljungström, E.; Hertervig, E.; Borgquist, R. Long-Term Outcomes of the Current Remote Magnetic Catheter Navigation Technique for Ablation of Atrial Fibrillation. *Scand. Cardiovasc. J.* **2017**, *51*, 308−315.
(23) Bauernfeind, T.; Akca, F.; Schwagten, B.; De Groot, N.; Van Belle, Y.; Valk, S.; Ujvari, B.; Jordaens, L.; Szili-Torok, T. The Magnetic Navigation System Allows Safety and High Efficacy for Ablation of Arrhythmias. *Europace* **2011**, *13*, 1015−1021.
(24) Carpi, F.; Pappone, C. Stereotaxis Niobe Magnetic Navigation System for Endocardial Catheter Ablation and Gastrointestinal Capsule Endoscopy. *Expert Rev. Med. Devices* **2009**, *6*, 487−498.
(25) Hennig, T. L.; Unterweger, H.; Lyer, S.; Alexiou, C.; Cicha, I. Magnetic Accumulation of SPIONs under Arterial Flow Conditions: Effect of Serum and Red Blood Cells. *Molecules* **2019**, *24*, 2588.
(26) Wu, S.; Hamel, C. M.; Qi, H. J.; Zhao, R.; et al.*et al.* Evolutionary Algorithm Guided Voxel-Encoding Printing of Functional Hard-Magnetic Soft Active Materials. *Adv. Intell. Syst.* **2020**, *2*, No. 2000060.
(27) Chen, Z.; Lin, Y.; Zheng, G.; Yang, Y.; Zhang, Y.; Zheng, S.; Li, J.; Li, J.; Ren, L.; Jiang, L. Programmable Transformation and Controllable Locomotion of Magnetoactive Soft Materials with 3D-Patterned Magnetization. *ACS Appl. Mater. Interfaces* **2020**, *12*, 58179−58190.
(28) Abbott, J. J.; Diller, E.; Petruska, A. J. Magnetic Methods in Robotics. *Annu. Rev. Control Rob. Auton. Syst.* **2020**, *3*, 57−90.
(29) Deng, H.; Sattari, K.; Xie, Y.; Liao, P.; Yan, Z.; Lin, J. Laser Reprogramming Magnetic Anisotropy in Soft Composites for Reconfigurable 3D Shaping. *Nat. Commun.* **2020**, *11*, No. 6325.
(30) Xu, T.; Zhang, J.; Salehizadeh, M.; Onaizah, O.; Diller, E. Millimeter-Scale Flexible Robots with Programmable Three-Dimensional Magnetization and Motions. *Sci. Rob.* **2019**, *4*, No. eaav4494.
(31) Ze, Q.; Kuang, X.; Wu, S.; Wong, J.; Montgomery, S. M.; Zhang, R.; Kovitz, J. M.; Yang, F.; Qi, H. J.; Zhao, R. Magnetic Shape Memory Polymers with Integrated Multifunctional Shape Manipulation. *Adv. Mater.* **2020**, *32*, No. 1906657.
(32) Kuang, X.; Wu, S.; Ze, Q.; Yue, L.; Jin, Y.; Montgomery, S. M.; Yang, F.; Qi, H. J.; Zhao, R. Magnetic Dynamic Polymers for Modular Assembling and Reconfigurable Morphing Architectures. *Adv. Mater.* **2021**, *33*, No. 2102113.
(33) Gu, H.; Boehler, Q.; Cui, H.; Secchi, E.; Savorana, G.; De Marco, C.; Gervasoni, S.; Peyron, Q.; Huang, T.-Y.; Pane, S.; Hirt, A. M.; Ahmed, D.; Nelson, B. J. Magnetic Cilia Carpets with Programmable Metachronal Waves. *Nat. Commun.* **2020**, *11*, No. 2637.
(34) Zhang, J.; Ren, Z.; Hu, W.; Soon, R. H.; Yasa, I. C.; Liu, Z.; Sitti, M. Voxelated Three-Dimensional Miniature Magnetic Soft Machines via Multimaterial Heterogeneous Assembly. *Sci. Rob.* **2021**, *6*, No. eabf0112.
(35) Kim, Y.; Genevriere, E.; Harker, P.; Choe, J.; Balicki, M.; Regenhardt, R. W.; Vranic, J. E.; Dmytriw, A. A.; Patel, A. B.; Zhao, X. Telerobotic Neurovascular Interventions with Magnetic Manipulation. *Sci. Rob.* **2022**, *7*, No. eabg9907.
(36) Hwang, J.; Jeon, S.; Kim, B.; Kim, J. Y.; Jin, C.; Yeon, A.; Yi, B. J.; Yoon, C. H.; Park, H. J.; Pané, S.; Nelson, B. J.; Choi, H. An Electromagnetically Controllable Microrobotic Interventional System for Targeted, Real-Time Cardiovascular Intervention. *Adv. Healthcare Mater.* **2022**, No. 2102529.
(37) Mahoney, A. W.; Abbott, J. J. Five-Degree-of-Freedom Manipulation of an Untethered Magnetic Device in Fluid Using a Single Permanent Magnet with Application in Stomach Capsule Endoscopy. *Int. J. Rob. Res.* **2016**, *35*, 129−147.
(38) Yang, Z.; Zhang, L. Magnetic Actuation Systems for Miniature Robots: A Review. *Adv. Intell. Syst.* **2020**, *2*, No. 2000082.
(39) Cui, J.; Kramer, M.; Zhou, L.; Liu, F.; Gabay, A.; Hadjipanayis, G.; Balasubramanian, B.; Sellmyer, D. Current Progress and Future Challenges in Rare-Earth-Free Permanent Magnets. *Acta Mater.* **2018**, *158*, 118−137.
(40) Shao, Z.; Ren, S. Rare-Earth-Free Magnetically Hard Ferrous Materials. *Nanoscale Adv.* **2020**, *2*, 4341−4349.
(41) Song, G.; Kenney, M.; Chen, Y. S.; Zheng, X.; Deng, Y.; Chen, Z.; Wang, S. X.; Gambhir, S. S.; Dai, H.; Rao, J. Carbon-Coated FeCo Nanoparticles as Sensitive Magnetic-Particle-Imaging Tracers with

https://doi.org/10.1021/acsami.2c04745
ACS Appl. Mater. Interfaces 2022, 14, 23896−23908

Photothermal and Magnetothermal Properties. *Nat. Biomed. Eng.* **2020**, *4*, 325−334.
(42) Liao, Z.; Hossain, M.; Yao, X.; Navaratne, R.; Chagnon, G. A Comprehensive Thermo-Viscoelastic Experimental Investigation of Ecoflex Polymer. *Polym. Test.* **2020**, *86*, No. 106478.
(43) Ning, N.; Li, S.; Wu, H.; Tian, H.; Yao, P.; HU, G. H.; Tian, M.; Zhang, L. Preparation, Microstructure, and Microstructure-Properties Relationship of Thermoplastic Vulcanizates (TPVs): A Review. *Prog. Polym. Sci.* **2018**, *79*, 61−97.
(44) Song, H.; Lee, H.; Lee, J.; Choe, J. K.; Lee, S.; Yi, J. Y.; Park, S.; Yoo, J. W.; Kwon, M. S.; Kim, J. Reprogrammable Ferromagnetic Domains for Reconfigurable Soft Magnetic Actuators. *Nano Lett.* **2020**, *20*, 5185−5192.
(45) Lu, H.; Zhang, M.; Yang, Y.; Huang, Q.; Fukuda, T.; Wang, Z.; Shen, Y. A Bioinspired Multilegged Soft Millirobot That Functions in Both Dry and Wet Conditions. *Nat. Commun.* **2018**, *9*, No. 3944.
(46) Crespi, A.; Badertscher, A.; Guignard, A.; Ijspeert, A. J. AmphiBot I: An Amphibious Snake-like Robot. *Rob. Auton. Syst.* **2005**, *50*, 163−175.
(47) Thorpe, S. K. S.; Holder, R. L.; Crompton, R. H. Origin of Human Bipedalism As an Adaptation for Locomotion on Flexible Branches. *Science* **2007**, *316*, 1328−1331.
(48) Alexander, R. M. *Principles of Animal Locomotion*; Princeton University Press, 2002.
(49) Heinrich, G.; Klüppel, M.; Vilgis, T. A. Reinforcement of Elastomers. *Curr. Opin. Solid State Mater. Sci.* **2002**, *6*, 195−203.
(50) Pak, O. S.; Gao, W.; Wang, J.; Lauga, E. High-Speed Propulsion of Flexible Nanowire Motors: Theory and Experiments. *Soft Matter* **2011**, *7*, 8169−8181.
(51) Wu, Y.; Yim, J. K.; Liang, J.; Shao, Z.; Qi, M.; Zhong, J.; Luo, Z.; Yan, X.; Zhang, M.; Wang, X.; Fearing, R. S.; Full, R. J.; Lin, L. Insect-Scale Fast Moving and Ultrarobust Soft Robot. *Sci. Rob.* **2019**, *4*, No. eaax1594.
(52) Mahoney, A. W.; Nelson, N. D.; Peyer, K. E.; Nelson, B. J.; Abbott, J. J. Behavior of Rotating Magnetic Microrobots above the Step-out Frequency with Application to Control of Multi-Microrobot Systems. *Appl. Phys. Lett.* **2014**, *104*, No. 144101.
(53) Huang, H.-W.; Uslu, F. E.; Katsamba, P.; Lauga, E.; Sakar, M. S.; Nelson, B. J. Adaptive Locomotion of Artificial Microswimmers. *Sci. Adv.* **2019**, *5*, No. eaau1532.
(54) Li, Z.; Myung, N. V.; Yin, Y. Light-Powered Soft Steam Engines for Self-Adaptive Oscillation and Biomimetic Swimming. *Sci. Rob.* **2021**, *6*, No. eabi4523.
(55) Hirt, M. R.; Jetz, W.; Rall, B. C.; Brose, U. A General Scaling Law Reveals Why the Largest Animals Are Not the Fastest. *Nat. Ecol. Evol.* **2017**, *1*, 1116−1122.
(56) Gogia, S.; Neelamegham, S. Role of Fluid Shear Stress in Regulating VWF Structure, Function and Related Blood Disorders. *Biorheology* **2016**, *52*, 319−335.
(57) Yang, Y.; Zhao, Y. Discretized Motion of Surface Walker under a Nonuniform AC Magnetic Field. *Langmuir* **2020**, *36*, 11125−11137.
(58) Qiu, Y.; Myers, D. R.; Lam, W. A. The Biophysics and Mechanics of Blood from a Materials Perspective. *Nat. Rev. Mater.* **2019**, *4*, 294−311.
(59) Jeon, G. H.; Kim, S. H. Development and Verification of Mechanism for Enhancement of Steering Angle and Active Locomotion for Magnetic Micro Active-Guidewire. *IEEE Access* **2020**, *8*, 31103−31113.
(60) Elsharawy, M.; Elzayat, E. Early Results of Thrombolysis vs Anticoagulation in Iliofemoral Venous Thrombosis. A Randomised Clinical Trial. *Eur. J. Vasc. Endovasc. Surg.* **2002**, *24*, 209−214.
(61) Kruger, P. C.; Eikelboom, J. W.; Douketis, J. D.; Hankey, G. J. Deep Vein Thrombosis: Update on Diagnosis and Management. *Med. J. Aust.* **2019**, *210*, 516−524.
(62) Weigandt, K.; N, W.; D, C.; E, E.; Y, W.; X, F.; DC, P. Fibrin Clot Structure and Mechanics Associated with Specific Oxidation of Methionine Residues in Fibrinogen. *Biophys. J.* **2012**, *103*, 2399−2407.
(63) Pitek, A. S.; Wang, Y.; Gulati, S.; Gao, H.; Stewart, P. L.; Simon, D. I.; Steinmetz, N. F. Elongated Plant Virus-Based Nanoparticles for Enhanced Delivery of Thrombolytic Therapies. *Mol. Pharmaceutics* **2017**, *14*, 3815−3823.
(64) Hu, J.; Huang, S.; Zhu, L.; Huang, W.; Zhao, Y.; Jin, K.; Zhuge, Q. Tissue Plasminogen Activator-Porous Magnetic Microrods for Targeted Thrombolytic Therapy after Ischemic Stroke. *ACS Appl. Mater. Interfaces* **2018**, *10*, 32988−32997.
(65) Zakharzhevskii, M. A.; Anastasova, E. I.; Kladko, D. V.; Prilepskii, A. Y.; Gorshkova, M. N.; Vinnik, D. A.; Taskaev, S. V.; Vinogradov, V. V. Shape Anisotropic Magnetic Thrombolytic Actuators: Synthesis and Systematic Behavior Study. *J. Mater. Chem. B* **2021**, *9*, 4941−4955.
(66) Tasci, T. O.; Disharoon, D.; Schoeman, R. M.; Rana, K.; Herson, P. S.; Marr, D. W. M.; Neeves, K. B. Enhanced Fibrinolysis with Magnetically Powered Colloidal Microwheels. *Small* **2017**, *13*, No. 1700954.
(67) Koupenova, M.; Kehrel, B. E.; Corkrey, H. A.; Freedman, J. E. Thrombosis and Platelets: An Update. *Eur. Heart J.* **2017**, *38*, 785−791.
(68) Zhao, Z.; Zhang, X. S. Topology Optimization of Hard-Magnetic Soft Materials. *J. Mech. Phys. Solids* **2022**, *158*, No. 104628.
(69) Wang, L.; Zheng, D.; Harker, P.; Patel, A. B.; Guo, C. F.; Zhao, X. Evolutionary Design of Magnetic Soft Continuum Robots. *Proc. Natl. Acad. Sci. U.S.A.* **2021**, *118*, No. e2021922118.
(70) Wang, L.; Kim, Y.; Guo, C. F.; Zhao, X. Hard-Magnetic Elastica. *J. Mech. Phys. Solids* **2020**, *142*, No. 104045.
(71) Baek, S. H.; Kim, S.; Kang, M.; Choi, J.-H.; Kwon, H. J.; Kim, D. W. Effect of Distal Access Catheter Tip Position on Angiographic and Clinical Outcomes Following Thrombectomy Using the Combined Stent-Retriever and Aspiration Approach. *PLoS One* **2021**, *16*, No. e0252641.

https://doi.org/10.1021/acsami.2c04745
ACS Appl. Mater. Interfaces 2022, 14, 23896−23908